AIAA JOURNAL
Vol. 32, No. 6, June 1994

Numerical Simulation of Turbulent Cylinder Juncture Flowfields

Donald P. Rizzetta*
Wright Laboratory, Wright-Patterson Air Force Base, Ohio 45433

Steady high-Reynolds-number subsonic and supersonic flowfields about a circular cylinder mounted upright on a flat plate were simulated numerically by integration of the time-dependent three-dimensional compressible mass-averaged Navier-Stokes equations. Effects of turbulence were represented by a two-equation (k-ε) closure model that included a generalized formulation and low-Reynolds-number terms. For the supersonic case, the turbulence equations incorporated a compressibility correction. Grid mesh step-size studies were performed to assess resolution requirements of the solutions. Comparison is made with experimental data in terms of static pressure and total pressure loss coefficients, velocity distributions, and surface limiting streamline patterns. The effect of the compressibility correction is also examined.

Nomenclature

C_{p_s} = static pressure coefficient, $2(p - p_0)/\rho_0 q_0^2$
C_{p_t} = total pressure loss coefficient, $2(p_{t_0} - p_t)/\rho_0 q_0^2$
d = cylinder diameter
h = cylinder height
k = turbulence kinetic energy
M_∞ = freestream Mach number
$\overline{N^+}$ = average number of grid points for which $y^+ < 10$
p = nondimensional static pressure
p_t = nondimensional total pressure
q = nondimensional velocity magnitude
Re = reference Reynolds number, $\rho_\infty u_\infty d/\mu_\infty$
r = radial distance normal to cylinder, $(x^2 + y^2)^{1/2}$
x, y, z = nondimensional Cartesian coordinates in streamwise, lateral, and vertical directions
x_{cp} = location of upstream critical point on plate surface at symmetry plane
y^+ = law-of-the-wall coordinate
$\overline{y^+}$ = average value of y^+ at first mesh point away from surface
α = compressibility correction coefficient (0.0 for subsonic, 1.0 for supersonic)
δ_0 = boundary-layer thickness at reference location
$\Delta\xi, \Delta\eta, \Delta\zeta$ = computational mesh step sizes
ε = turbulence energy dissipation
ξ, η, ζ = computational coordinates
θ = circumferential angle
ρ = nondimensional fluid density

Subscripts
min = minimum value
0 = evaluated at reference location $x = -2.72$, $y = 0.0$, $z = 0.5h/d$

Introduction

WHEN the fluid flowing over a flat plate immersed in a subsonic or supersonic stream encounters a circular cylinder mounted upright on the surface, the adverse pressure gradient induced by the presence of the obstacle produces separation of the boundary layer and formation of a horseshoe system consisting of one or more primary vortices. These vortices wrap themselves around the cylinder, spiraling downstream, and may be accompanied by the appearance of secondary counter-rotating flow. Such structures provide a mechanism for the removal of the low-energy fluid that accumulates in the separated region near the cylinder/plate junction and contain concentrated vorticity that decays slowly as they are convected downstream. This configuration not only characterizes a fundamental flowfield that exhibits three-dimensional separation and its associated intricate fluid phenomena but also is representative of the juncture flows that occur in a wide variety of practical circumstances, including wing/fuselage and wing/pylon intersections, struts of aerospace vehicles, submarine conning towers, turbomachinery, wind-tunnel model supports, architectural aerodynamics, and meteorological and geological applications.

Because of the inherently interesting nature of juncture flowfields, extensive experimental investigations have been conducted to understand their basic features.[1-12] These studies have considered cylindrical and winglike protuberances, subsonic and supersonic regimes, and laminar and turbulent flow conditions. More recently, three-dimensional numerical simulations of such flows have been performed[13-21] that have focused principally on the low-speed laminar situation and have been able to elucidate aspects of the flows that were not previously possible. The computations by Chen and Patel,[15] Chima and Yokota,[17] and Chen and Hung[21] have attempted to numerically reproduce turbulent juncture flows. A wing-body intersection in subsonic flow was calculated by Chen and Patel[15] using a two-equation model to simulate turbulence. The solution employed a rather coarse computational mesh, and the turbulence model was degenerated to a single equation in near-wall regions. Chima and Yokota[17] and Chen and Hung[21] utilized a standard algebraic turbulence model to compute the subsonic flow past a vertical blunt flat plate and the supersonic flow past a cylinder/plate combination, respectively. As is customary with algebraic closures, an ad hoc modification to the turbulence model was necessary to account for the multiple intersecting solid surfaces.

The objective of the present investigation is to numerically simulate both subsonic and supersonic high-Reynolds-number cylinder juncture flowfields. Effects of turbulence are represented by an eddy viscosity coefficient that is prescribed as a function of the turbulence kinetic energy k and its corresponding dissipation rate ε. For this purpose, the generalized

Received July 1, 1993; presented as Paper 93-3038 at the AIAA 24th Fluid Dynamics Conference, Orlando, FL, July 6-9, 1993; revision received Oct. 29, 1993; accepted for publication Nov. 6, 1993.

*Aerospace Engineer, CFD Research Branch, Aeromechanics Division. Associate Fellow AIAA.

compressible formulation due to Gerolymos[22] is employed, which incorporates low-Reynolds-number terms to model near-wall effects. For supersonic flows, the compressibility correction proposed by Sarkar et al.[23] has also been adopted. The two-equation model requires no predefined turbulence length scales or wall functions, and because of the inclusion of the low-Reynolds-number terms, homogeneous conditions for both k and ε may be applied along solid surfaces. Thus, the formulation is attractive for generating practical solutions of flowfields about complex three-dimensional configurations, for applications employing unstructured computational meshes, or for numerical results obtained on massively parallel computing machines having distributed memory multiprocessing architectures.

It is the purpose of these calculations to determine the utility of the k-ε equations for the practical simulation of turbulent cylinder/plate juncture flowfields by direct comparison with experiment. Grid mesh step-size studies were performed to assess resolution requirements of the solutions. The numerical procedure is summarized, and the effect of the compressibility correction is examined. Numerical results are compared with existing experimental data in terms of static pressure and total pressure loss coefficients, velocity distributions, and surface limiting streamline patterns.

Governing Equations

The governing equations were taken to be the unsteady compressible three-dimensional Navier-Stokes equations written in nondimensional mass-averaged variables. Effects of turbulence were accounted for by specifying a turbulent Prandtl number of 0.9 and by incorporating a two-equation model for the turbulence kinetic energy k and the turbulence dissipation rate ε. The k-ε equations were originally devised by Jones and Launder[24] for the computation of incompressible boundary-layer flows and were subsequently modified by including low-Reynolds-number terms to improve near-wall modeling.[25] This formulation was considered to perform well in the comprehensive comparative study conducted by Patel et al.[26]

The choice of the specific k-ε model was motivated by the fact that the Cartesian tensor form of the equations is directly applicable to three spatial dimensions and does not require the use of any predefined length scales. Furthermore, because the equation for ε is formulated in terms of the difference between the dissipation of the turbulent kinetic energy and the dissipation of homogeneous turbulence, homogeneous boundary conditions for both k and ε may be applied at solid surfaces, thereby facilitating the computation of flows about geometrically complex configurations. The governing equations are essentially identical to those that have been successfully applied by Gerolymos[22] for the computation of transonic channel flowfields, by Rizzetta[27] for the simulation of supersonic slot injection, and by Rizzetta and Visbal[28] for the calculation of airfoil static and dynamic stall.

The complete form of the governing equations appears in Ref. 29. In addition, the Sutherland law for the molecular viscosity coefficient and the perfect gas relationship were employed, and Stokes' hypothesis for the bulk viscosity coefficient has been invoked. A coefficient α was utilized as an artifice to either include or exclude the compressibility correction from the turbulent kinetic energy equation.

Numerical Procedure

Solutions to the governing equations were obtained numerically using the implicit approximately factored finite difference algorithm of Beam and Warming[30] to advance the computational flowfield to a steady state. First-order Euler implicit time differencing was employed along with second-order accurate central-difference approximations for all spatial derivatives. Common forms of both implicit and explicit nonlinear dissipation[31] were utilized to augment stability, with the pressure gradient parameter given according to Vatsa[32] in the supersonic case. Nominal values of user-defined damping coefficients were assigned, and the dissipation was scaled by the square of the local velocity magnitude so that it essentially vanished in regions adjacent to solid boundaries. The k-ε equations were temporally decoupled from the mean flow equations by lagging their values by one time step from the other dependent variables. In addition, k and ε were uncoupled from each other by also evaluating the vector source term explicitly from the previous time step. Thus only scalar tridiagonal matrix inversions were required for implicit solution of either the k or ε equation.

An existing fully vectorized time-accurate three-dimensional Navier-Stokes code was modified according to the method described here to accommodate solution of the k-ε equations. The code has proven to be reliable for a variety of both steady and unsteady fluid flow problems.[16,18,19,33–37] To further increase efficiency, the implicit portion of the factorized equations was solved in diagonalized form.[38]

Several meshes, whose parameters may be found in Table 1, were generated for both the supersonic and subsonic cases to facilitate grid resolution studies. An extensive description of the computations, including specification of the boundary conditions, generation of the computational meshes, details of the time-marching procedure, and results of the grid resolution study, may be found in Ref. 29. It was not in general possible to investigate the effect of numerical damping on all solutions because of the computational resources involved. On the coarsest grids, however, solutions remained invariant when the nominal damping coefficients were increased by a factor of 2.

Results

The configuration to be considered consists of a circular cylinder of diameter d and height h mounted upright on a flat surface and is depicted schematically in Fig 1. A Cartesian coordinate system is oriented with its origin located at the intersection of the cylinder axis of symmetry and the plane of the plate as indicated. Flow conditions and dimensions of the cylinder geometries are given in Table 2. Unless noted otherwise, all of the results described here correspond to solutions obtained on the finest grids.

Supersonic Flowfield

The numerical calculation simulated the experiment of Sedney and Kitchens,[1,2] for the flow indicated in Table 2, who tested cylinders of various height-to-diameter ratios. Those experiments established that, for the case investigated here, the cylinder could be considered to be infinite in length[2] with regard to the horseshoe vortex system. Previously, Chen and Hung[21] performed a similar computation of this same case, employing algebraic turbulence modeling and a two-block grid, and described many of its topological features.

Presented in Fig. 2 are some of the major features of the supersonic cylinder/plate juncture flowfield. Color contours correspond to levels of constant total pressure on the upstream plane of symmetry. Because of the displacement effect of the separated region, a weak oblique shock is produced that intersects the primary shock upstream of the cylindrical surface to produce the classic "λ" pattern that is exhibited in the figure. Superimposed on these contours are streamlines at the plane of symmetry. Path lines of particles forming the primary and secondary horseshoe vortex systems appear in red. As viewed from the figure, the primary vortex spirals in the clockwise direction, out from the plane of symmetry, whereas the secondary vortex rotates in the opposite direction. Below these are limiting streamlines on the plate surface that delineate separation of the primary vortex and attachment of the secondary vortex. It is noted that in this supersonic case the primary vortex is rather flat in shape and lies at a greater distance upstream of the cylinder than will be seen subsequently for subsonic flow.

Table 1 Computational mesh parameters

Case	Mesh size	$\Delta\xi_{min}$	$\Delta\eta_{min}$	$\Delta\zeta_{min}$	$\overline{y^+}$	$\overline{N^+}$
Supersonic	(191 × 131 × 81)	2.18×10^{-3}	1.00×10^{-4}	1.00×10^{-4}	0.969	9
	(144 × 99 × 61)	2.90×10^{-3}	1.34×10^{-4}	1.50×10^{-4}	1.294	7
	(96 × 66 × 41)	4.36×10^{-3}	2.05×10^{-4}	2.12×10^{-4}	1.700	5
Subsonic	(191 × 141 × 81)	2.18×10^{-3}	1.00×10^{-4}	1.00×10^{-4}	1.850	6
	(144 × 106 × 61)	2.90×10^{-3}	1.34×10^{-4}	1.50×10^{-4}	2.318	5
	(96 × 71 × 41)	4.36×10^{-3}	2.05×10^{-4}	2.05×10^{-4}	2.711	4

Table 2 Flow conditions

Case	M_∞	Re	d, cm	h, cm
Supersonic	2.5	7.3533×10^5	3.81	10.16
Subsonic	0.083	5.5×10^5	29.85	30.48

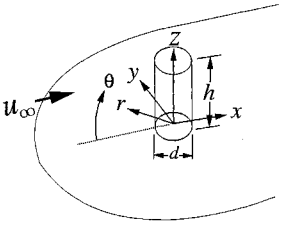

Fig. 1 Cylinder/plate juncture geometry.

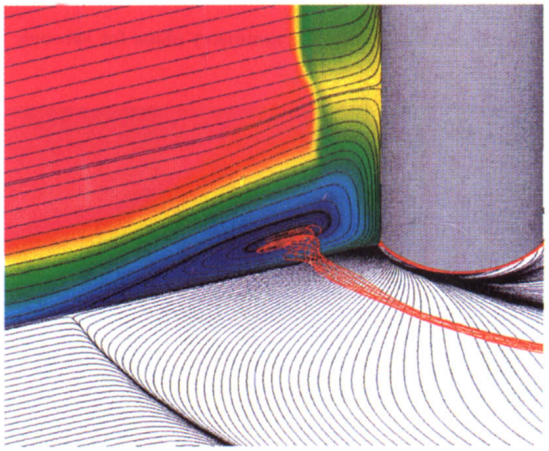

Fig. 2 Limiting streamline patterns, total pressure contours, and particle paths for supersonic flowfield.

Comparison between the numerical solution and experimental data[2] appears in Fig. 3 in terms of the limiting streamline pattern on the plate surface as viewed from above. The experimental result was obtained from a shadow photograph such that the shock wave and Mach stem are visible upstream of the cylinder but do not appear in the numerical figure, which shows only surface values. Location of the upstream critical point on the plate surface at the plane of symmetry, x_{cp}, is provided in Table 3. The present fine-grid calculation incorporating a compressibility correction ($\alpha = 1.0$) is seen to compare well with the experimentally observed value. As the grid is refined, x_{cp} moves upstream because the shock is numerically strengthened with increasing resolution, thereby enlarging the separated flow region. Although the current result compares better with the experiment than that of Chen and Hung,[21] their computational mesh was somewhat coarser. At the cylinder leading edge, it appears that the numerical solution underpredicts the extent of the observed secondary flow region. It can also be seen that the computation differs

Table 3 Location of upstream critical point for supersonic flowfield

Case	Mesh size	x_{cp}
$\alpha = 1.0$	(96 × 66 × 41)	−2.361
$\alpha = 1.0$	(144 × 99 × 61)	−2.433
$\alpha = 1.0$	(191 × 131 × 81)	−2.451
$\alpha = 0.0$	(191 × 131 × 81)	−2.188
Experiment[2]	——	−2.4
Chen and Hung[21]	(103 × 77 × 45) plus (10 × 44 × 45)	−2.28

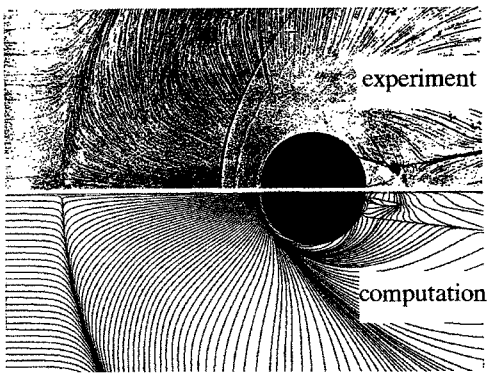

Fig. 3 Comparison between experimental and computed limiting streamline patterns on plate surface for supersonic flowfield.

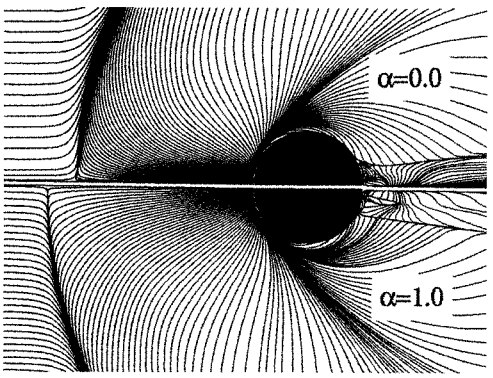

Fig. 4 Effect of compressibility correction on limiting streamline patterns on plate surface for supersonic flowfield.

from the experiment in the near-wake region. Some of this disparity may be attributed to a lack of numerical resolution behind the cylinder, since this was not the area of primary focus, and no effort was made to thoroughly refine this region.

The effect of the compressibility correction is visible in Fig. 4 where limiting streamline patterns on the plate surface are compared for solutions both with ($\alpha = 1.0$) and without ($\alpha = 0.0$) its inclusion. Omission of the term is observed to decrease the extent of the interaction region as noted by the location of the line of separation (see Table 3). This was identical to the behavior for the simulation of slot injection into a supersonic stream.[27] The figure also shows that the

compressibility correction has a pronounced effect on the solution in the region downstream of the cylinder.

Subsonic Flowfield

The subsonic calculations attempt to numerically reproduce the experiment of Eckerle and Langston[4,7] for the flow conditions given in Table 1. Profiles of velocity magnitude and total pressure loss coefficient for several spanwise stations at the most upstream data measuring location are compared with experimental results in Figs. 5 and 6, respectively. The calculated velocities appear to agree better with the data at the plane of symmetry ($y = 0.0$) than they do outboard. This may be attributed to decreasing resolution away from $y = 0.0$. It is unclear why the experimental measurements fail to approach the inviscid limit ($q/q_0 = 1.0$) at the midheight of the wind tunnel ($z = 0.511$). Computed values of the total pressure loss coefficient agree well with the data at all spanwise stations as shown in Fig. 6.

Figure 7 presents streamline patterns at the plane of symmetry from numerical solutions generated on each of three different computational grids. Although the flow topological structure is not central to the present effort, some interesting features are apparent. In particular, for the coarsest grid (96 × 71 × 41) no vortex formation occurred, except very near the cylinder/plate juncture. On the other two grids, however, a large vortex is evident and is only slightly stronger on the finest mesh.

Streamlines for the fine-grid calculation are shown in more detail in Fig. 8, where arrowheads and color shading have been added to help elucidate the flow topology. The boundary-layer thickness at the upstream reference location is indicated by δ_0. Each individual color identifies flow emanating from a distinguished vertical region of the upstream flowfield. Designations noted in the figure are "N" for the spiral node, "S" for the saddle point, and "N_A'" for the half-node of attachment. Fluid regions colored red and green denote the flow that at the plate surface is separated upstream and downstream, respectively, by the half-node of attachment. Yellow represents the fluid region forming the primary vortex, whereas that of the secondary vortex is shown in blue. This structure is fundamentally different from that of the supersonic case, for which the upstream critical point is a half-saddle of separation. A more complete discussion of various topologies that are possible for juncture flowfields may be found in Refs. 18–21.

General features of the subsonic flowfield are illustrated in Fig. 9. As in the supersonic case, streamlines on the plane of symmetry are superimposed over color contours of constant total pressure. In the absence of shock waves, the total pressure is seen to remain constant along streamlines in those portions of the flowfield that are essentially inviscid. Particle paths of the primary and secondary vortices appear in red.

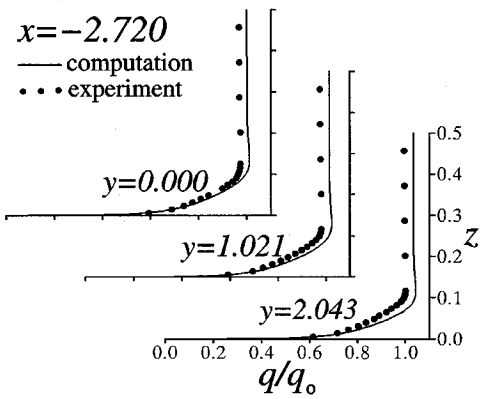

Fig. 5 Velocity profiles upstream of juncture for subsonic flowfield.

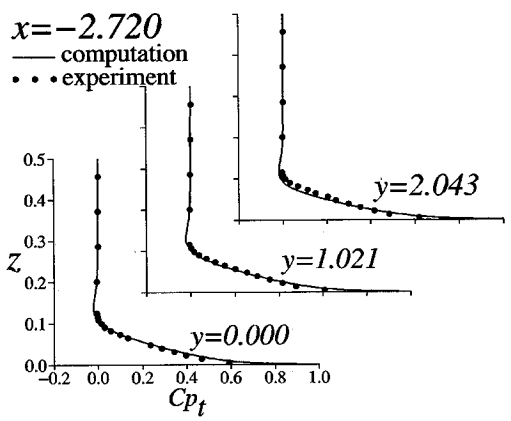

Fig. 6 Total pressure loss profiles upstream of juncture for subsonic flowfield.

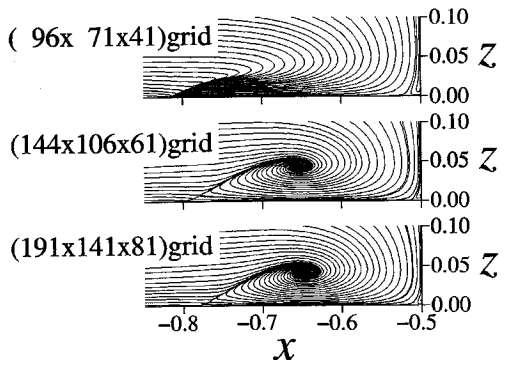

Fig. 7 Effect of grid resolution on streamline patterns at the symmetry plane for subsonic flowfield.

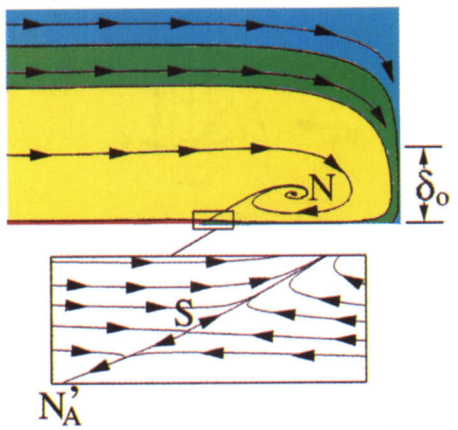

Fig. 8 Streamline patterns at the symmetry plane for subsonic flowfield.

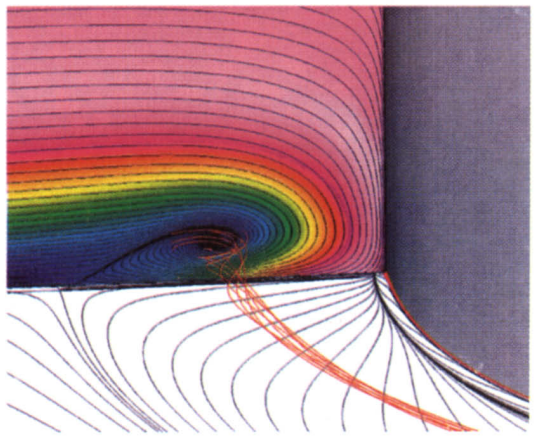

Fig. 9 Limiting streamline patterns, total pressure contours, and partical paths for subsonic flowfield.

Plate surface limiting streamlines show the line of coalescence upstream of the primary vortex, as well as the line of divergence upstream of the secondary. As alluded to earlier, the vortex in this instance is more round, diffuse, and weaker than in the supersonic case (see Fig. 2).

Computed and experimentally observed limiting streamline patterns on the plate surface are compared in Fig. 10. The location of the numerically derived line of coalescence is seen to lie much closer to the cylinder than does its experimental counterpart. Table 4 quantifies the location of the upstream critical point on the plate surface at the plane of symmetry as a function of grid size. As the grid is refined, it is noted that x_{cp} moves closer to the cylinder. The reason for this is that as the numerical vortex forms and strengthens with increasing resolution, more low-momentum fluid accumulating in the juncture region can be entrained by the vortex and convected downstream, thereby relieving some of the viscous displacement effect.

Static pressure contours on the plate surface as viewed from above are displayed in Fig. 11, where the "footprint" of the vortex can be observed upstream of the cylinder. Effects of the vortex lie closer to the cylinder for the computational results. Overall, however, the comparison is favorable. Near the shoulder of the cylinder (θ = 90 deg) some disparity is visible and is probably due to increasing coarseness of the circumferential mesh. In Fig. 12, static pressure contours are displayed on the unwrapped surface of the cylinder. Relatively good agreement is evident except near the plate surface in the region of the shoulder.

Table 4 Location of upstream critical point for subsonic flowfield

Mesh size	x_{cp}
(96 × 71 × 41)	−0.820
(144 × 106 × 61)	−0.799
(191 × 141 × 81)	−0.782
Experiment[4]	−0.88

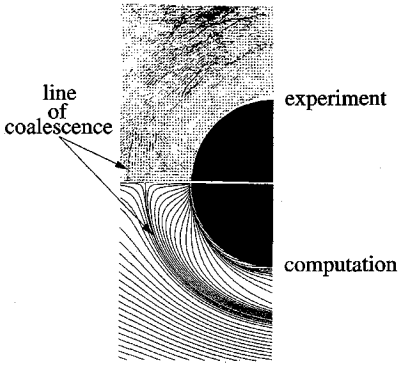

Fig. 10 Comparison between experimental and computed limiting streamline patterns on plate surface for subsonic flowfield.

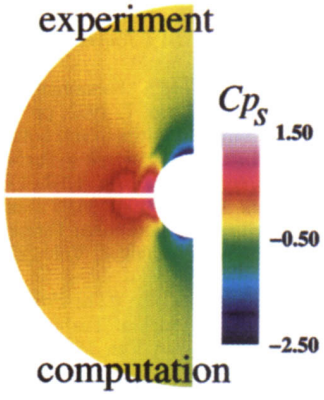

Fig. 11 Comparison between experimental and computed static pressure contours on plate surface for subsonic flowfield.

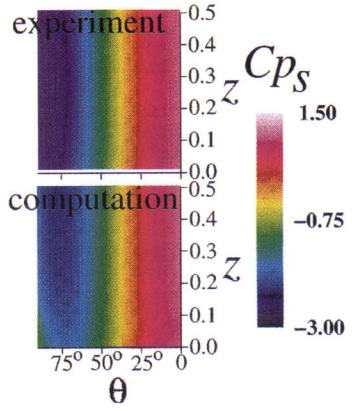

Fig. 12 Comparison between experimental and computed static pressure contours on cylinder surface for subsonic flowfield.

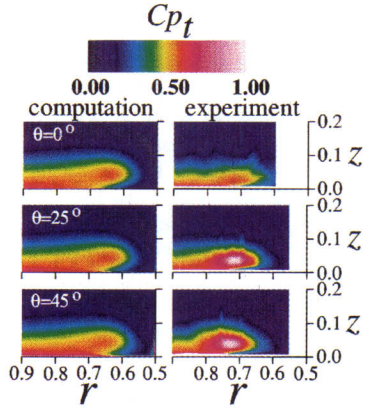

Fig. 13 Comparison between experimental and computed total pressure loss survey contours for subsonic cylinder.

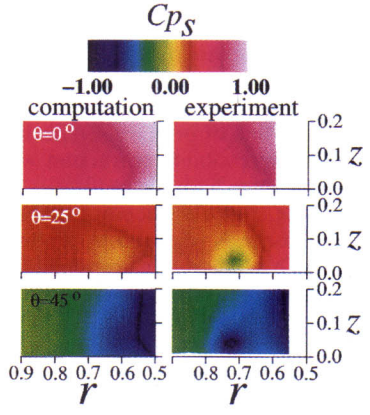

Fig. 14 Comparison between experimental and computed static pressure survey contours for subsonic cylinder.

Figures 13–15 present comparisons of the computed solution with experimental data in radial/vertical planes at various circumferential locations. Because of limitations of the measuring equipment (five-hole probe), data were not obtained fully either to the cylinder (r = 0.5) or to the plate surface (z = 0.0), as will be apparent in the figures. Surveys of the total pressure loss coefficient are indicated in Fig. 13. The computation is seen to predict a vortex located at the same vertical distance above the plate but at a smaller radial distance from the cylinder than that of the experiment. Although the strength and size of the computed vortex are virtually invariant with θ, the data reveal an increase in both size and strength away from the plane of symmetry. A similar behavior is inferred from the static pressure surveys in Fig.

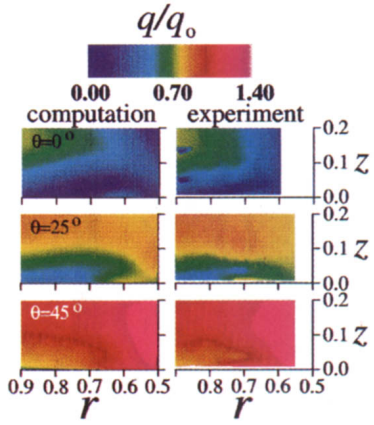

Fig. 15 Comparison between experimental and computed velocity survey contours for subsonic cylinder.

14. At $\theta = 45$ deg, the calculated contours indicate diffusiveness in the vortex core. Low pressure is produced in this region as the flow expands around the cylinder. Velocity magnitudes are exhibited in Fig. 15. Here, the comparison is generally good. Once again, at $\theta = 45$ deg the expansion generates very high velocities. Note that the viscous layer near $z = 0.0$ for $\theta = 45$ deg is quite thin.

As a whole, the comparisons in Figs. 13–15 are qualitatively favorable. Some disparity resulted due to decreasing resolution away from the plane of symmetry, thus precluding fidelity in the convection of vorticity around the cylinder. Poor numerical prediction of the vortex location is probably a consequence of the turbulence modeling. In this regard, however, it is felt that this particular flow situation may be quite sensitive to a number of parameters, both numerical and physical.

Summary and Conclusions

Steady high-Reynolds-number flows about cylinder/plate junctures were computed employing a two-equation (k-ε) model to simulate effects of turbulence. All commonly observed physical features of the flowfields were duplicated by the calculations. For the supersonic case, the numerical result reproduced the experimentally generated surface streamline pattern, including the line of primary separation at the plate surface. Use of a compressibility correction was determined to be essential toward this end.

In the subsonic case, a grid refinement study indicated that considerable resolution was required to produce the correct vortical structure. This might be accomplished more efficiently with the use of a multiblock and/or grid adaptive technique. Velocity and pressure loss profiles upstream of the cylinder were adequately predicted by the computation. The flow topological structure at the plane of symmetry indicated that the upstream critical point on the plate surface was a half-node of attachment as opposed to a half-saddle of separation, which is more common.

Reasonable agreement between the numerical solution and experimental data was found for pressure distributions on the plate and cylinder surfaces, as well as for surveys of pressure loss, static pressure, and velocity magnitude. The major deficiency of the calculations was some loss of grid resolution for increasing θ and an inability to correctly predict the vortex strength and location. This not withstanding, the k-ε equations appear to provide a practical means for the simulation of flows past complicated geometries or for those that possess an inherently complex fluid nature.

Acknowledgments

Computational resources for the work presented here were provided through the auspices of the Air Force Super Computer Center, Eglin Air Force Base, Florida, and the Air Force Super Computer Center, Kirtland Air Force Base, New Mexico. The author is grateful to M. R. Visbal for helping to identify much of the cited literature and experimental database, as well as for a number of helpful discussions.

References

[1]Sedney, R., and Kitchens, C. W., "The Structure of Three-Dimensional Separated Flows in Obstacle, Boundary-Layer Interactions," AGARD-CP-168, No. 37, May 1975, pp. 1–15.

[2]Sedney, R., and Kitchens, C. W., "Separation Ahead of Protuberances in Supersonic Turbulent Boundary Layers," Ballistic Research Lab., Rept. 1958, Aberdeen Proving Ground, MD, Feb. 1977.

[3]Baker, C. J., "The Laminar Horseshoe Vortex," *Journal of Fluid Mechanics*, Vol. 95, Pt. 2, 1979, pp. 347–367.

[4]Eckerle, W. A., and Langston, L. S., "Measurements of a Turbulent Horseshoe Vortex Formed Around a Cylinder," NASA Contractor Rept. 3986, June 1986.

[5]Kubendran, L. R., McMahon, H. M., and Hubbartt, J. E., "Turbulent Flow Around a Wing/Fuselage-Type Juncture," *AIAA Journal*, Vol. 24, No. 9, 1986, pp. 1447–1452.

[6]Thomas, A. S. W., "The Unsteady Characteristics of Laminar Juncture Flow," *Physics of Fluids*, Vol. 30, No. 2, 1987, pp. 283–285.

[7]Eckerle, W. A., and Langston, L. S., "Horseshoe Vortex Formation Around a Cylinder," *Journal of Turbomachinery*, Vol. 109, No. 2, 1987, pp. 278–285.

[8]Kubendran, L. R., Bar-Sever, A., and Harvey, W. D., "Flow Control in a Wing/Fuselage-Type Juncture," AIAA Paper 88-0614, Jan. 1988.

[9]Pierce, F. J., and Harsh, M. D., "The Mean Flow Structure Around and Within a Turbulent Junction or Horseshoe Vortex—Part II: The Separated and Junction Vortex Flow," *Journal of Fluids Engineering*, Vol. 110, No. 4, 1988, pp. 415–423.

[10]Devenport, W. J., and Simpson, R. L., "Time-Dependent and Time-Averaged Turbulence Structure near the Nose of a Wing-Body Junction," *Journal of Fluid Mechanics*, Vol. 210, Jan. 1990, pp. 23–55.

[11]Angui, J., and Andreopoulos, J., "Experimental Investigation of a Three-Dimensional Boundary Layer Flow in the Vicinity of an Upright Wall Mounted Cylinder," AIAA Paper 90-1545, June 1990.

[12]Fleming, J. L., Simpson, R. L., and Devenport, W. J., "An Experimental Study of a Turbulent Wing-Body Junction and Wake Flow," AIAA Paper 92-0434, Jan. 1992.

[13]Kaul, U. K., Kwak, D., and Wagner, C., "A Computational Study of Saddle Point Separation and Horseshoe Vortex System," AIAA Paper 85-0182, Jan. 1985.

[14]Briley, W. R., Buggelin, R. C., and McDonald, H., "Solution of the Three-Dimensional Navier-Stokes Equations for a Steady Laminar Horseshoe Vortex Flow," AIAA Paper 85-1520, July 1985.

[15]Chen, H. C., and Patel, V. C., "The Flow Around Wing-Body Junctions," Fourth Symposium on Numerical and Physical Aspects of Aerodynamic Flows, Long Beach, CA, Jan. 1989.

[16]Visbal, M. R., "Numerical Investigation of Laminar Juncture Flows," AIAA Paper 89-1873, June 1989.

[17]Chima, R. V., and Yokota, J. W., "Numerical Analysis of Three-Dimensional Viscous Internal Flows," *AIAA Journal*, Vol. 28, No. 5, 1990, pp. 798–806.

[18]Visbal, M. R., "The Laminar Horse Vortex System Formed at a Cylinder/Plate Juncture," AIAA Paper 91-1826, June 1991.

[19]Visbal, M. R., "Structure of Laminar Juncture Flows," *AIAA Journal*, Vol. 29, No. 8, 1991, pp. 1273–1282.

[20]Hung, C. M., Sung, C. H., and Chen, C. L., "Computation of Saddle Point of Attachment," *AIAA Journal*, Vol. 30, No. 6, 1992, pp. 1561–1569.

[21]Chen, C. L., and Hung, C. M., "Numerical Study of Juncture Flows," *AIAA Journal*, Vol. 30, No. 7, 1992, pp. 1800–1807.

[22]Gerolymos, G. A., "Implicit Multiple-Grid Solutions of the Compressible Navier-Stokes Equations Using k-ε Turbulence Closure," *AIAA Journal*, Vol. 28, No. 10, 1990, pp. 1707–1717.

[23]Sarkar, S., Erlebacher, G., Hussaini, M. Y., and Kreiss, H. O., "The Analysis and Modelling of Dilatational Terms in Compressible Turbulence," *Journal of Fluid Mechanics*, Vol. 227, June 1991, pp. 473–493.

[24]Jones, W. P., and Launder, B. E., "The Prediction of Laminarization with a Two-Equation Model of Turbulence," *International Journal of Heat and Mass Transfer*, Vol. 15, No. 2, 1972, pp. 301–314.

[25]Jones, W. P., and Launder, B. E., "The Calculation of Low-Reynolds-Number Phenomena with a Two-Equation Model of Turbulence," *International Journal of Heat and Mass Transfer*, Vol. 16,

No. 6, 1973, pp. 1119–1130.

[26]Patel, V. C., Rodi, W., and Scheuerer, G., "Turbulence Models for Near-Wall and Low Reynolds Number Flows: A Review," *AIAA Journal*, Vol. 23, No. 9, 1985, pp. 1308–1319.

[27]Rizzetta, D. P., "Numerical Simulation of Slot Injection into a Turbulent Supersonic Stream," *AIAA Journal*, Vol. 30, No. 10, 1992, pp. 2434–2439.

[28]Rizzetta, D. P., and Visbal, M. R., "Comparative Numerical Study of Two Turbulence Models for Airfoil Static and Dynamic Stall," *AIAA Journal*, Vol. 31, No. 4, 1993, pp. 784–786.

[29]Rizzetta, D. P., "Numerical Simulation of Turbulent Cylinder Juncture Flowfields," AIAA Paper 93-3038, July 1993.

[30]Beam, R., and Warming, R., "An Implicit Factored Scheme for the Compressible Navier-Stokes Equations," *AIAA Journal*, Vol. 16, No. 4, 1978, pp. 393–402.

[31]Jameson, A., Schmidt, W., and Turkel, E., "Numerical Solutions of the Euler Equations by Finite Volume Methods Using Runge-Kutta Time Stepping Schemes," AIAA Paper 81-1259, June 1981.

[32]Vatsa, V. N., "Evaluation of a Multigrid-Based Navier-Stokes Solver for Aerothermodynamic Computations," AIAA Paper 92-4563, Aug. 1992.

[33]Webster, W. P., and Shang, J. S., "Thin-Layer Full Navier-Stokes Simulations over a Supersonic Delta Wing," *AIAA Journal*, Vol. 29, No. 9, 1991, pp. 1363–1369.

[34]Gordnier, R. E., and Visbal, M. R., "Unsteady Navier-Stokes Solutions for a Low Aspect Ratio Delta Wing," AIAA Paper 90-1538, June 1990.

[35]Gordnier, R. E., and Visbal, M. R., "Numerical Simulation of the Unsteady Vortex Structure over a Delta Wing," AIAA Paper 91-1811, June 1991.

[36]Webster, W. P., and Shang, J. S., "Numerical Simulation of Vortex Breakdown Over a Subsonic Delta Wing," AIAA Paper 91-1814, June 1991.

[37]Stanek, M. J., and Visbal, M. R., "Investigation of Vortex Development on a Pitching Slender Body of Revolution," AIAA Paper 91-3273, Sept. 1991.

[38]Pulliam, T. H., and Chaussee, D. S., "A Diagonal Form of an Implicit Approximate-Factorization Algorithm," *Journal of Computational Physics*, Vol. 39, No. 2, 1981, pp. 347–363.